

Delivery of Stimulator of Interferon Genes (STING) Agonist Using Polypeptide-Modified Dendrimer Nanoparticles in the Treatment of Melanoma

Pere Dosta, Alexander M. Cryer, Michaela Prado, Michelle Z. Dion, Shiran Ferber, Santhosh Kalash, and Natalie Artzi*

The activation of stimulator of interferon genes (STING) in the cytosol by cyclic dinucleotides (CDNs) enhances antitumor immunity through the induction of proinflammatory cytokines, such as type-I interferons (IFN-I). However, the high hydrophilicity and negative charge of CDNs hinders their delivery into cells. Here, by developing a library of cationic polypeptide-modified dendrimers, it is shown that CDNs can be efficiently delivered intracellularly *in vitro* and *in vivo*. With respect to naked dendrimers, generation-5 polyamidoamine (G5-PAMAM) dendrimers modified with arginine or with a mixture of arginine/lysine polypeptides affords higher CDN-packaging capacity and leads to higher activation of IFN-I and the nuclear factor kappa-light-chain-enhancer of activated B cells (NF- κ B) proinflammatory signaling pathway. In the B16-F10 murine model of melanoma, the intratumoral administration of a synthetic CDN via arginine-modified G5-PAMAM dendrimers at a low dose induces strong antitumor responses and inhibits tumor growth. It is also shown that the combination of this therapy with immune checkpoint blockade (ICB) further improves the therapeutic outcomes. Cationic polypeptide dendrimers may be advantageous in the delivery of gene-based immunomodulators for the treatment of solid tumors.

1. Introduction

Using the innate immune system to instigate an antitumor response is an increasingly attractive approach in cancer immunotherapy. Engagement of pathogen-associated molecular patterns (PAMPs) with their respective pattern recognition receptors (PRRs) was reported to elicit robust downstream endogenous cytokine production and immune cell activation,^[1] which is responsible for the potent immune responses generated by vaccines and against tumors. Cyclic dinucleotides (CDNs), such as the second messenger 2'3'-cyclic guanosine monophosphate-adenosine monophosphate (cGMP-AMP or cGAMP), are a class of PAMPs that are generated upon sensing cytosolic DNA.^[2] The production of cGAMP leads to agonism of stimulator of interferon genes (STING),^[3] enacting a type-I interferon (IFN-I)-driven proinflammatory program including the stimulation of

dendritic cells (DCs) and cross-presentation of tumor antigens to T-cells, thereby priming them for antitumor effector functionality.^[4] This bridge between innate and adaptive antitumor immunity positions STING as a critical regulator of immunosurveillance, reinforced by studies in STING-deficient mice highlighting increased susceptibility to tumorigenesis and diminished responsiveness to immunotherapy such as immune checkpoint inhibitors (ICIs).^[5]

The role of STING signaling in antitumor responses as well as insufficient endogenous agonism has prompted investigations into exogenous cGAMP and structural analogs as therapeutics to promote antitumor immunity.^[6] Intratumoral (IT) injection of CDNs has reached phase I clinical trials;^[7] however, CDNs are anionic and highly hydrophilic, which restricts their entry into the cytoplasm where STING resides.^[8] Consequently, CDNs have transient interactions with immune cells (e.g., DCs, macrophages) in the tumor microenvironment (TME) and are rapidly eliminated from the tumor site.

Biomaterial-based delivery strategies can be leveraged to improve internalization into cells, therefore augmenting the activity of adjuvants such as STING agonists.^[9] Indeed, it has previously been demonstrated that using nanoparticles (NPs) of lipidic^[10] or polymeric^[11] origin to encapsulate CDNs can

Dr. P. Dosta, Dr. A. M. Cryer, M. Prado, M. Z. Dion, Dr. S. Ferber, Dr. S. Kalash, Dr. N. Artzi
Institute for Medical Engineering and Science
Massachusetts Institute of Technology
Cambridge, MA 02139, USA
E-mail: nartzi@mit.edu, nartzi@bwh.harvard.edu

Dr. P. Dosta, Dr. A. M. Cryer, M. Prado, M. Z. Dion, Dr. S. Ferber, Dr. S. Kalash, Dr. N. Artzi
Department of Medicine
Division of Engineering in Medicine
Brigham and Women's Hospital
Harvard Medical School
Boston, MA 02115, USA

 The ORCID identification number(s) for the author(s) of this article can be found under <https://doi.org/10.1002/anbr.202100006>.

© 2021 The Authors. Advanced NanoBiomed Research published by Wiley-VCH GmbH. This is an open access article under the terms of the Creative Commons Attribution License, which permits use, distribution and reproduction in any medium, provided the original work is properly cited.

DOI: 10.1002/anbr.202100006

improve their antitumor activity. However, liposomes suffer from poor packaging capacity and limited storage stability and the encapsulation of small hydrophilic molecules within polymeric NPs remains challenging.^[12] We reasoned that stable electrostatic complexes could be formed between anionic CDNs and cationic NPs, which would act to improve their stability, cytosolic localization, and endosomal escape, resulting in greater antitumor responses.

Dendrimers have an established history as drug delivery vehicles^[13] and have been used in immunotherapy as accessories in antibody–drug conjugates or in vaccine formulations.^[14] Polyamidoamine (PAMAM) dendrimers are hyperbranched polymers consisting of tertiary amines throughout the dendrimer core and terminal primary amines, the number of which increases with each layer of branching, known as a generation.^[15] This defined architecture yields cationic, low-polydispersity NPs with many surface-reactive sites per NP. It has been noted that highly localized cationicity is not well tolerated on a cellular level,^[16] with the external primary amines being the principal drivers of this toxicity. Therefore, we leveraged the reactivity of these amines to functionalize dendrimers with basic polypeptide motifs consisting of arginine, lysine, or histidine. By replacing external amines with biocompatible amino acids, the cytotoxicity is significantly attenuated, cellular internalization and transfection efficiency are improved, and endosomal escape can be better controlled.^[17] In addition, it has been demonstrated that these polypeptides can influence the nanoparticle composition, allowing the design of cell-specific nanoparticle formulations.^[18] Endowed with these properties, we hypothesized that polypeptide-functionalized dendrimers could effectively complex with CDNs and be internalized by immune cells, enhancing CDN activity *in vitro* and *in vivo*. We investigated the physicochemical properties of the polypeptide-modified dendrimers, their ability to deliver the synthetic CDN ADU-S100 to immune cells, biocompatibility, cellular uptake, and antitumor efficacy *in vivo*, as well as the associated immune responses.

2. Results

2.1. Synthesis of Polypeptide-Modified Dendrimers

We developed a library of dendrimers with diverse surface modifications using cationic polypeptides that can complex with CDNs and form a wide range of NPs with distinct physicochemical properties. Synthesis of polypeptide-conjugated dendrimers was performed via a two-step reaction. First, the PAMAM G5 dendrimer was modified with a bifunctional succinimidyl-[(*N*-maleimidopropionamido)-diethyleneglycol]-ester linker [SM(PEG)₂] by conjugating the primary dendrimer amines to the succinimidyl group. Then, the modified dendrimers were conjugated with cationic polypeptide moieties through sulfhydryl–maleimide conjugation of the thiol group of cysteine-terminated polypeptides to the maleimide group of the SM(PEG)₂ linker, obtaining around 79 peptides per dendrimer (Figure 1A and Figure S9, Supporting Information). Polypeptide-modified dendrimers were purified by dialysis and their molecular structure characterized by ¹H-NMR. The chemical structure of the resultant dendrimers was confirmed

by the presence of signals associated with the conjugated polypeptides (Figure S1–S8, Supporting Information).

To assess the effect of the polypeptides on our dendrimer formulations, size (hydrodynamic diameter) and surface charge values were obtained using dynamic light scattering (DLS) and zeta potential measurements, respectively (Figure 1). Whereas the unmodified dendrimers were small (5.47 ± 0.05 nm) and positively charged (14.77 ± 6.32 mV), the end-modified dendrimers were larger, ranging from 7 to 10 nm, and those modified with arginine (D-CR3), lysine (D-CK3), and a mixture of lysine/histidine (D-K/H) and arginine/lysine (D-R/K) showed an increase in surface charge compared to nonmodified dendrimers (ranging from +24 mV to +31 mV). In contrast, dendrimers modified with histidine (D-CH3) or a mixture of histidine/arginine (D-R/H) were less positive ($\approx +10$ mV) than nonmodified dendrimers ($\approx +15$ mV). In addition, when the dendrimer was only modified with a bifunctional SM(PEG)₂ linker (without polypeptides), the zeta potential was markedly more negative (-7.07 ± 0.34 mV). The addition of different polypeptides can be used to tune the final nanoparticle surface charge, ranging from neutral to positive.

2.2. Formulation and Biophysical Characterization of Polypeptide-Modified Dendrimers

The CDN complexation efficacy of the newly synthesized dendrimers was evaluated by agarose gel electrophoresis at different dendrimer/CDN ratios (w/w) (Figure 2 and Figure S10, Supporting Information). A fluorescently labeled CDN [termed CDN-F; c-(Ap-8-Fluo-AET-Gp)] was used to assess the complexation efficiency. Complexes prepared with unmodified dendrimer and fluorescent CDN (CDN-F) revealed free CDN-F at ratios below 64:1 dendrimer:CDN-F (w/w), while at a ratio of 64:1 complete CDN-F complexation was observed. D-CR3 showed complete CDN-F retardation at 16:1 D-CR3/CDN-F ratios, suggesting a more efficient complexation of CDN-F (0.5 CDN-F molecules per unmodified dendrimer vs 2 CDN-F molecules per D-CR3). In contrast, D-CK3 required dendrimer-to-CDN-F ratios similar to unmodified PAMAM dendrimer to achieve full CDN-F complexation. Moreover, D-CH3 was not able to complex the CDN-F at any of the tested ratios (Figure S10, Supporting Information). These results suggest that, compared to unmodified PAMAM dendrimer, D-CR3 significantly increases the number of CDN molecules per dendrimer NP, whereas dendrimers modified with lysine and histidine polypeptides contain a similar or lower number of CDN molecules per dendrimer NP than the unmodified dendrimer.

2.3. In Vitro Selection of Polypeptide-Modified Dendrimer for Efficient ADU-S100 Delivery

Given the importance of interferon regulatory factor (IRF)3 and nuclear factor (NF)- κ B in efficient STING signaling, we assessed the ability of functionalized dendrimers to deliver ADU-S100 and stimulate IRF3 and NF- κ B responses in human monocytic THP-1 Dual cells (Figure 3). THP-1 Dual cells allow the simultaneous study of the IRF3 pathway, by assessing the activity of a secreted luciferase, and the NF- κ B pathway, by monitoring

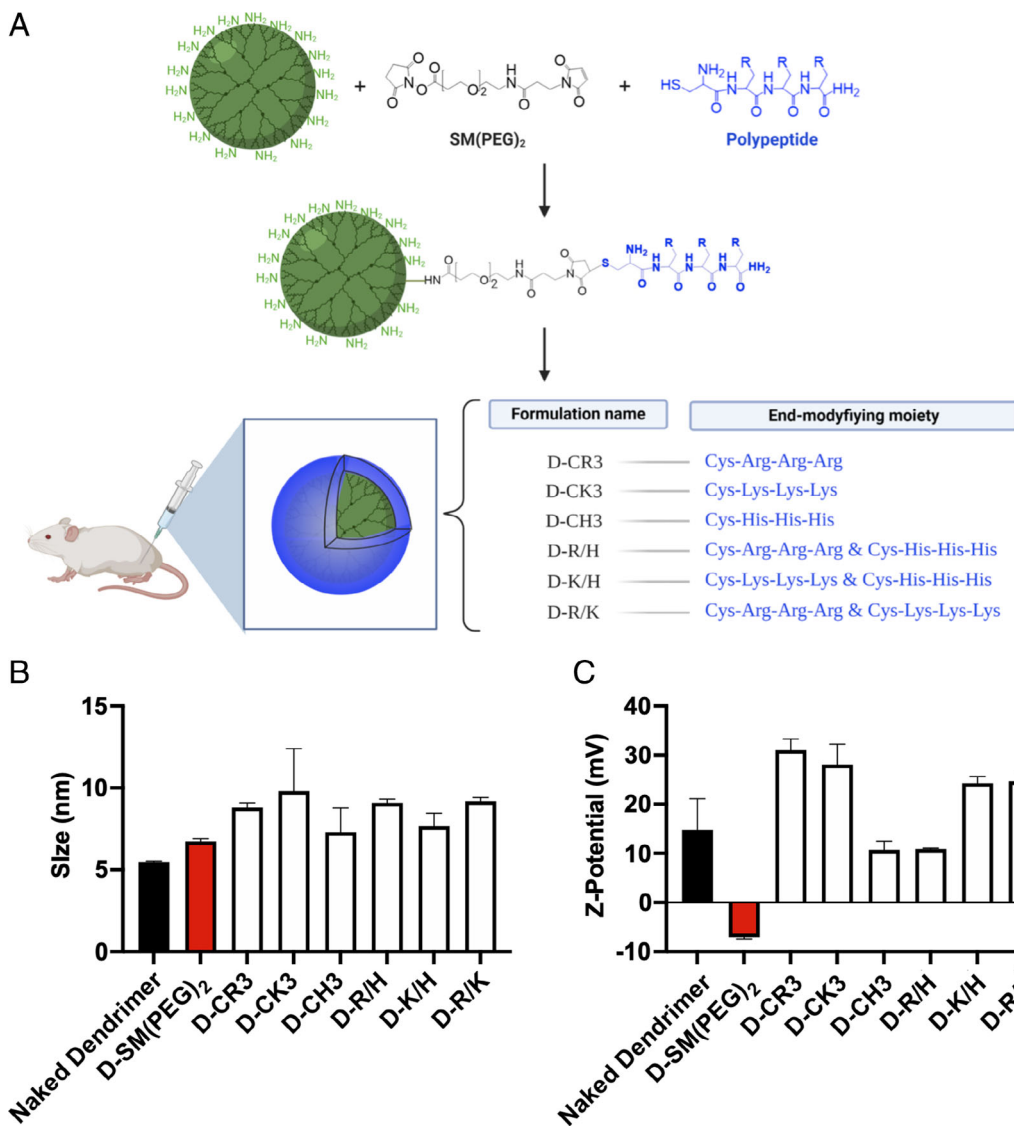


Figure 1. Synthesis and characterization of polypeptide-modified dendrimers. A) Different polypeptides were used for the synthesis of a new family of end-modified dendrimers (arginine-modified dendrimer, D-CR3; lysine-modified dendrimer, D-CK3; histidine-modified dendrimer, D-CH3; 50% arginine–50% histidine modified dendrimer, D-R/H; 50% lysine–50% histidine modified dendrimer, D-K/H; and 50% arginine–50% lysine modified dendrimer, D-R/K). B) Size (determined by DLS) and (C) Z-potential measurements of end-modified dendrimers ($n = 3$); data shown as mean \pm SD.

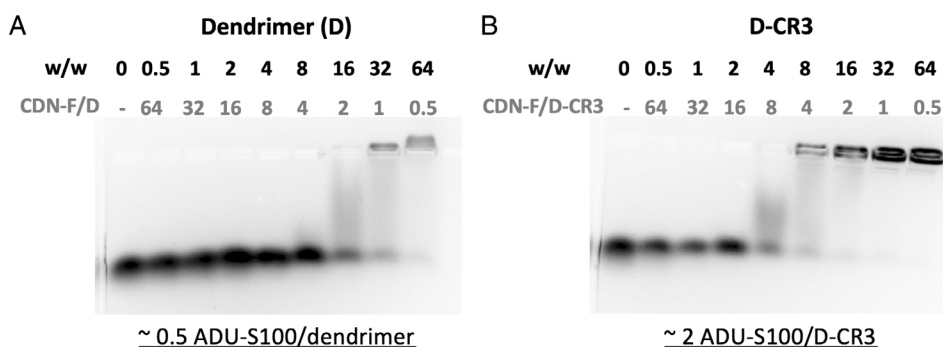


Figure 2. Agarose retardation assay of polypeptide-modified dendrimer–CDN-F polyplexes. Polyplexes were formed using CDN-F and different polypeptide-modified dendrimers at indicated w/w ratios and loaded onto an agarose gel to assess CDN-F mobility by electrophoresis for A) nonmodified dendrimer and B) D-CR3 formulation.

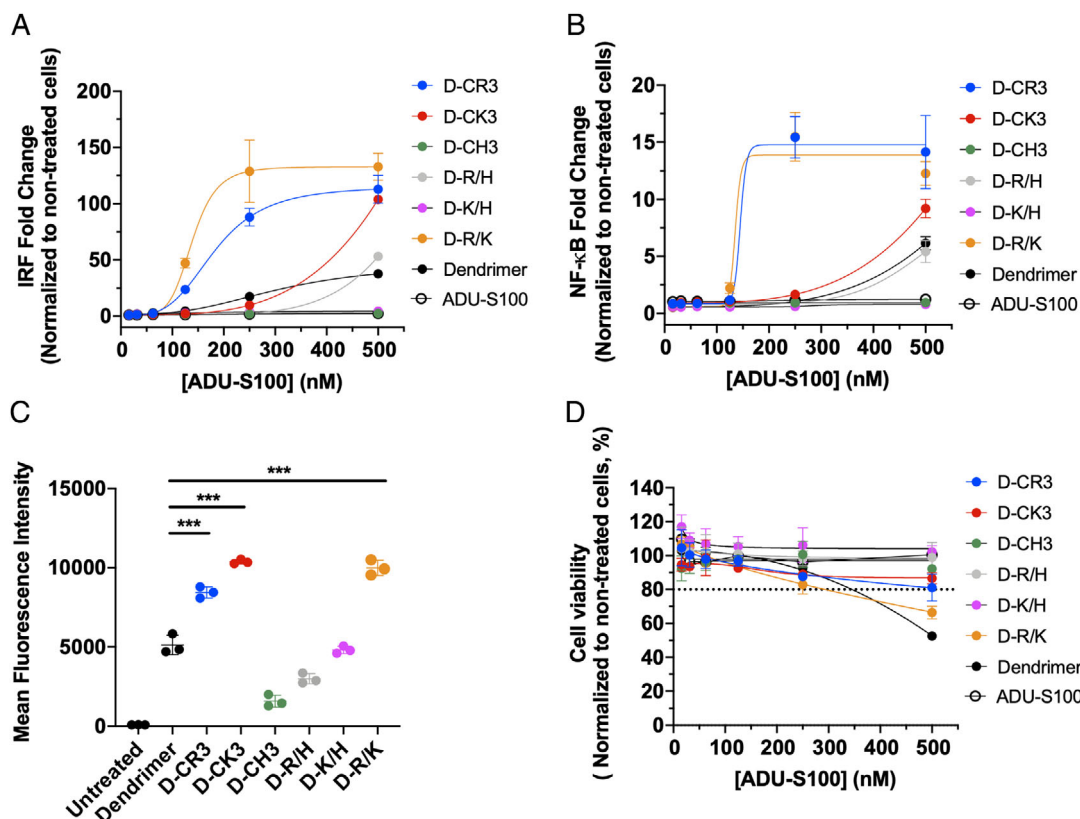


Figure 3. In vitro screening of polypeptide-modified dendrimers. A,B) Potent IRF3 and NF-κB activation following CDN delivery using polypeptide-modified dendrimers. The polypeptide-modified dendrimers were screened for A) IRF3 activation and B) NF-κB activation using THP-1 Dual cells. Cells were treated with different concentrations of ADU-S100 prior to measuring IRF3 and NF-κB 24 h posttreatment. Values were normalized to untreated cells. C) Cell internalization efficiency of polypeptide-modified dendrimers in THP-1 Dual cells. Cells were treated with polypeptide-modified dendrimers containing ADU-S100 at the final concentration of 125 nM, and fluorescence expression per cell was determined 2 h posttransfection by flow cytometry. D) Cell viability of different concentrations of polypeptide-modified dendrimers was analyzed 24 h posttreatment. Samples were normalized to untreated cells. Data are represented as mean ± SD ($n = 3$). Multiple comparisons among groups were determined using one-way ANOVA followed by a Fisher's LSD test. P -value: * $p < 0.05$, ** $p < 0.01$, *** $p < 0.001$.

the activity of secreted embryonic alkaline phosphatase (SEAP). D-CR3 and D-R/K achieved higher IRF3 activation than the unmodified dendrimer. In contrast, D-CH3 or D-K/H showed the lowest level of activation, similar to that of free ADU-S100. D-CK3 or D-R/H showed high IRF3 activation at higher ADU-S100 doses (500 nM). A similar trend was seen in terms of NF-κB activation for all formulations (Figure 3B). A 16-fold NF-κB increase was observed when ADU-S100 was delivered using either the D-CR3 or D-R/K formulation at 250 nM. In contrast, no NF-κB activation was detected when D-CH3 or D-K/H was used, and NF-κB expression was only detected at high ADU-S100 doses when D-CK3 and D-R/H formulations were used. In addition, we did not observe activation of IRF3 or NF-κB in STING-deficient THP-1 Dual cells (Figure S12, Supporting Information).

To determine if cellular internalization could account for the differences in IRF3 and NF-κB, uptake of polypeptide-modified dendrimers was assessed in THP-1 cells (Figure 3C). Dendrimers were fluorescently labeled, and their uptake was quantified by flow cytometry. We confirmed that formulations showing high IRF3 activation exhibited higher cellular internalization than those with low IRF3 activation. D-CR3, D-CK3, and

D-R/K were more efficiently internalized than the unmodified dendrimer and D-CH3 and D-R/H showed the lowest internalization. More than 90% of the cells showed nanoparticle uptake for all of the dendrimer formulations, except those of the D-CH3 formulation. Interestingly, D-CK3 was efficiently internalized, but less potent IRF3 activation was observed compared to D-CR3 and D-R/K. This can stem from the fact that less CDN is delivered per (Figure S10, Supporting Information). An increase in the number of dendrimer surface amines in the case of D-CK3 can enhance its internalization. However, its lysine residues have a lower pKa than arginine in D-CR3, which will impart weaker electrostatic interactions between the D-CK3 and the CDN compared to that with D-CR3.

To ensure the biocompatibility of functionalized dendrimers, the viability of THP-1 cells was determined 24 h post ADU-S100 delivery using our library of dendrimer formulations (Figure 3D). The cell viability of the polypeptide-modified dendrimers was higher than that of unmodified dendrimers at a CDN concentration of 500 nM, suggesting that the addition of natural peptides can increase the biocompatibility of dendrimer NPs. D-CR3 and D-R/K, which were highly efficient at delivering ADU-S100, showed different cell viability profiles. While D-CR3

cell viability was greater than 80%, the D-R/K formulation showed some toxicity at high CDN concentrations (500 nM). Taking that into account, we selected the D-CR3 formulation to deliver ADU-S100 in vivo.

2.4. IT Delivery of ADU-S100 with D-CR3 NPs Inhibits B16-10 Tumor Growth and Increases Survival

The recent approval of different checkpoint inhibitor therapies for the treatment of immunogenic tumors has opened the door to the treatment of different cancers; however, the development of more efficacious therapies is still needed. Recently, it has been demonstrated that ICIs antibodies, such as antiprogrammed cell death protein 1 (anti-PD-1), have a synergistic effect with STING agonist therapies.^[19] Here, we assessed whether combination therapy with D-CR3 NPs complexed with ADU-S100 (termed D-CR3-ADU) and anti-PD-1 showed a significant benefit compared to free ADU-S100 alone or D-CR3-ADU NPs alone in a syngeneic subcutaneous murine melanoma model. ADU-S100 therapy (0.5 µg per dose) was initiated when the tumor volume reached 100 mm³ and was delivered intratumorally (IT) four times, every 4 days, over the course of 12 days. Anti-PD-1 was administered via intraperitoneal injection, in the combination therapy groups, 24 h after ADU-S100 delivery (four injections, every 4 days). Tumor size was monitored every other day (Figure 4A). Control tumors treated with phosphate buffered saline (PBS) injection grew rapidly, whereas tumors treated with ADU-S100-containing formulations showed delayed tumor growth (Figure 4B). D-CR3-ADU-treated mice showed slower

tumor growth and increased survival when compared to ADU-S100. The combination of D-CR3-ADU and anti-PD-1 significantly inhibited tumor growth compared to ADU-S100 alone. A similar trend was observed when free ADU-S100 was combined with anti-PD-1, where reduced tumor growth and improved survival were observed. However, the NP-based delivery of ADU-S100, D-CR3 NPs, further inhibited tumor growth and enhanced survival compared to the free drug form.

2.5. IT Delivery of CDN Modifies the Immune Profile of the Tumor Microenvironment

To understand the mechanism by which the D-CR3 formulation containing ADU-S100 resulted in enhanced antitumor activity, we conducted immunohistochemical analysis of the TME 7 days after delivery of the last IT dose (19 days after treatment initiation) (Figure 5). We found that tumors treated with D-CR3-ADU have less actively proliferating cells [determined by hematoxylin and eosin (H&E) and Ki-67 staining] compared to tumors treated with free ADU-S100, which is further reduced when D-CR3-ADU is combined with anti-PD-1. In addition, infiltration of CD8⁺ T-cells and upregulation of the immune checkpoint molecule PD-L1 on tumor cells were observed when tumors were treated with D-CR3-ADU compared to untreated tumors or those treated with free ADU-S100. Similar results were obtained for the combination with anti-PD-1 compared to D-CR3-ADU alone.

Next, we conducted immunophenotyping of the TME and tumor-draining lymph node (tdLN) 3 days after a single IT injection of ADU-S100, with or without D-CR3 complexation,

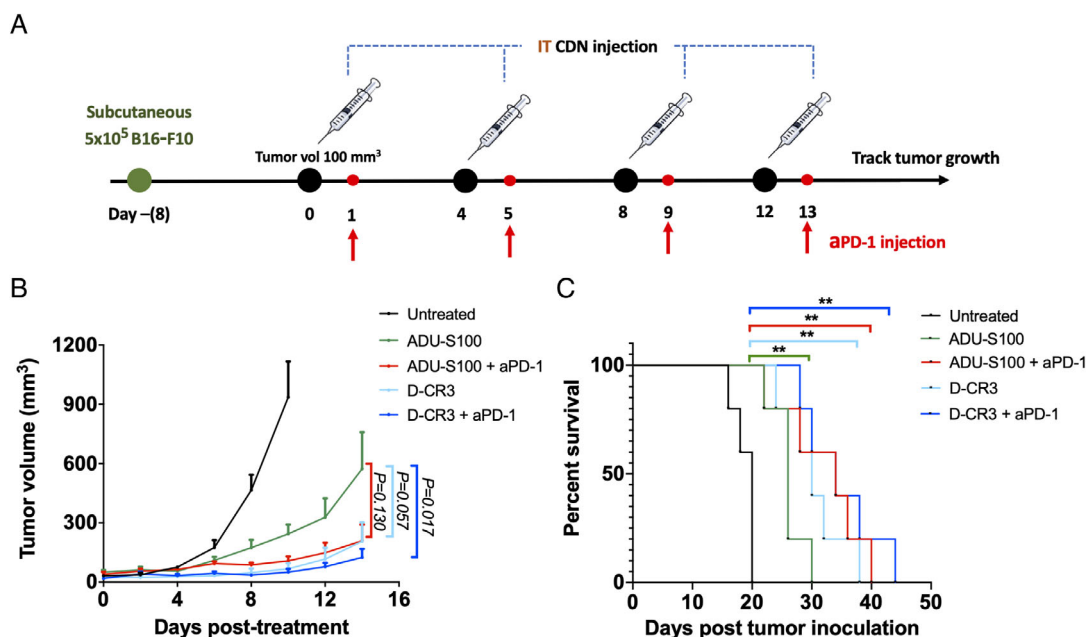


Figure 4. D-CR3-CDN polyplex therapy reduces tumor growth and increases animal survival, which is further enhanced when combined with anti-PD-1. A) Study design of subcutaneous B16-F10 model. NP administration was initiated 8 days following tumor induction, when the tumor size reached 100 mm³. Intraperitoneal administration of anti-PD-1 was performed 24 h post NP administration. B) Tumor growth was monitored every other day after the first administration. 0.5 µg of ADU-S100 delivered with D-CR3 NP, with and without anti-PD-1, resulted in statistically reduced tumor burden compared to free ADU-S100. Data are represented as mean ± SD (*n* = 5). Multiple comparisons among groups were determined using uncorrected Dunn's test. C) Kaplan–Meier survival curves of mice treated with the indicated formulation using a 1000 mm³ tumor volume or poor body condition as the endpoint criterion. Statistical analysis (*n* = 5) was performed using a log-rank Mantel–Cox test.

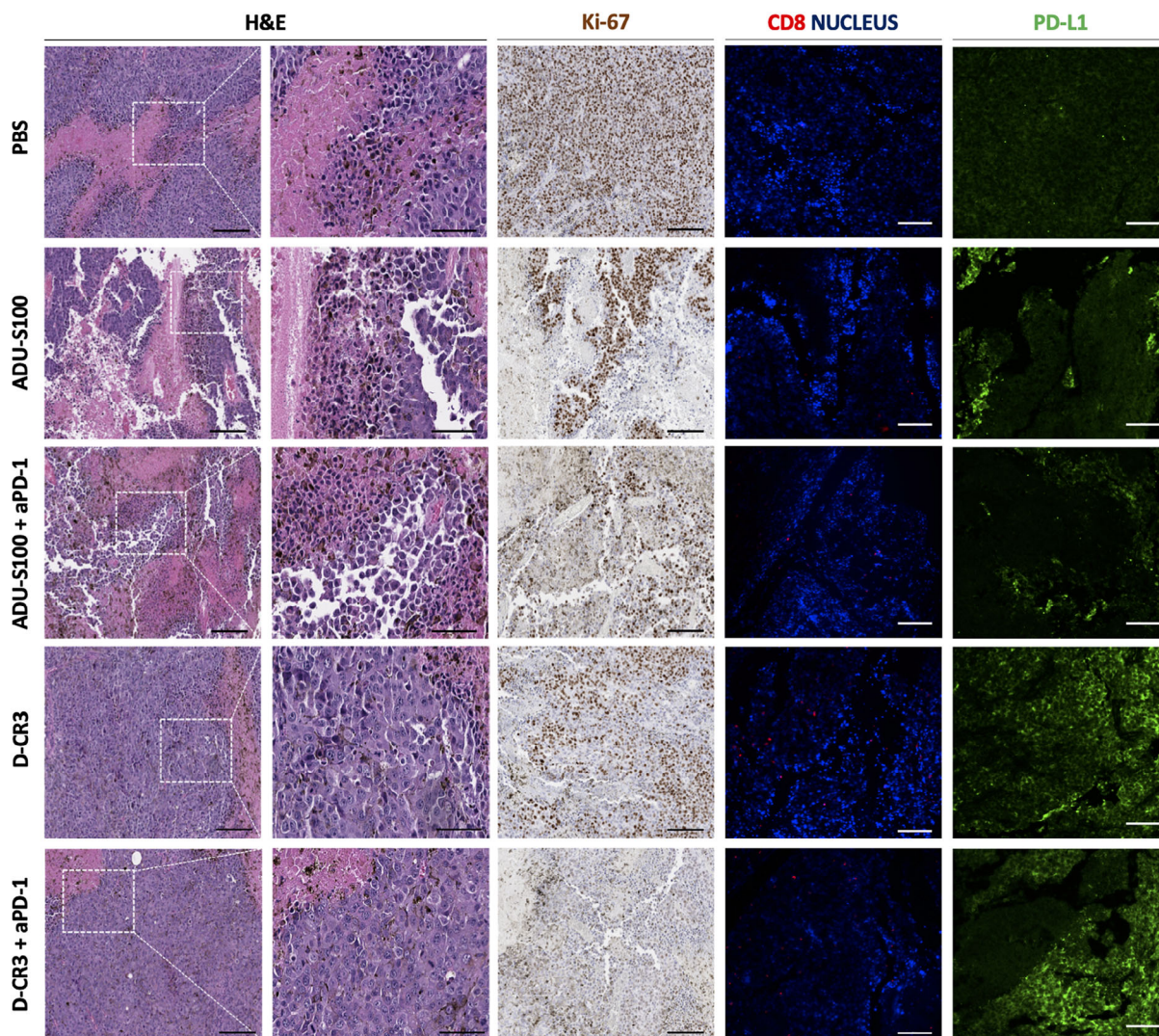


Figure 5. D-CR3-ADU polyplex therapy reduces cancer cell proliferation, increases CD8⁺ cytotoxic T-cell infiltration and PD-L1 cancer cell expression. Representative H&E staining (left, scale bar: 100 μ m; right: scale bar: 50 μ m), Ki-67 staining (scale bar: 100 μ m), immunofluorescence staining of CD8⁺ T-cells (red, CD8; blue, DAPI; scale bar: 100 μ m), and PD-L1⁺ cancer cells (PD-L1⁺, green; scale bar: 100 μ m) in tumors harvested on day 19.

as well as with or without anti-PD-1 combination therapy. Flow cytometry analysis of tumoral immune infiltrates (Figure 6A) revealed an increase in the CD8⁺/CD4⁺ T-cell ratio—a common prognostic biomarker of responsiveness to immunotherapy^[20]—in the D-CR3-ADU-treated groups, compared to untreated and to free-ADU-S100-treated tumors. We also witnessed a slight increase in the CD8⁺/*T*_{reg} (defined as CD4⁺FOXP3⁺) ratio in tumors treated with D-CR3-ADU and anti-PD-1 and a trend towards an increased presence of tumor-infiltrating T-cells (Figure 6B). Remarkably, the number of NK cells was higher in all treated groups compared to untreated tumors, but significantly more in the tumors treated with D-CR3-ADU. A significant increase in activated granulocytic cells (CD11b⁺Gr-1⁺, which includes monocytes, neutrophils, eosinophils, and myeloid-derived suppressor cells) was seen in all treatment groups (Figure 6C). Moreover, increased expression of the DCs activation marker CD86 was observed within the TME in all

the treated groups, compared to untreated tumors (Figure 6D). Interestingly, DC infiltration in the tdLN was elevated in all the treatment groups, with D-CR3-ADU in combination with aPD-1 having the highest DC expression (Figure 6E). Also, higher PD-1 expression was observed in CD8⁺ and CD4⁺ cells in the tdLN when ADU-S100 was delivered with a D-CR3 NP (Figure 6F–G).

3. Discussion

The generation of endogenous CDNs in response to cytoplasmic double-stranded DNA is an evolutionarily conserved innate immune defense mechanism, resulting in the production of IFN-I. Traditionally recognized as a response to viral infection, this process has been increasingly implicated in antitumor immunity.^[21] Indeed, the potency of CDNs spurred efforts to produce structural analogs of the endogenous adjuvant

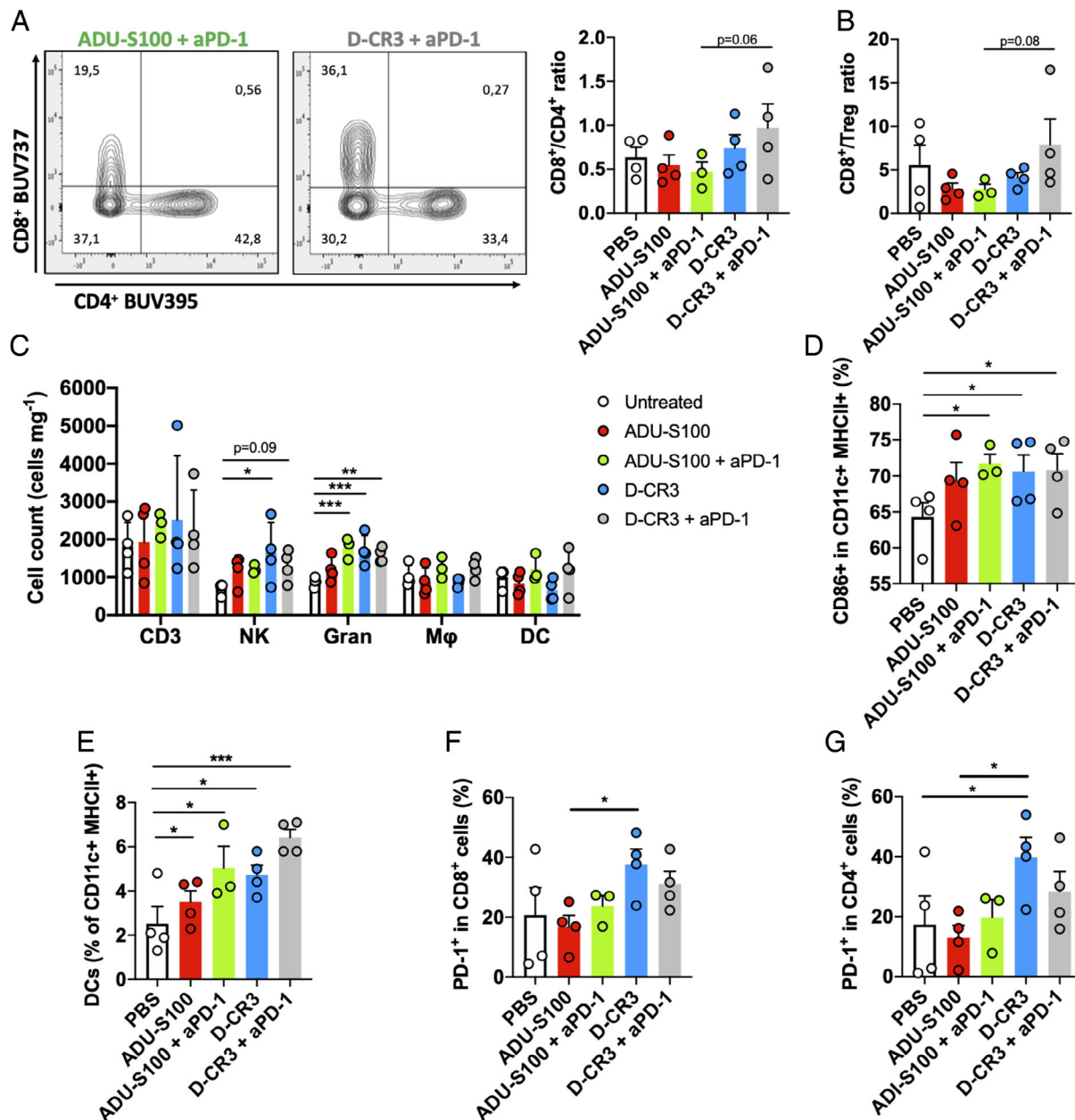


Figure 6. IT delivery of the D-CR3-CDN polyplex shifts the immune TME composition. A) Representative flow cytometry dot plot and quantification of tumor-infiltrating CD4⁺ and CD8⁺ T cells' ratio. B) Ratio of CD8⁺ to Tregs cells in the TME. C) Flow cytometric quantification of the number of lymphocytes cells (CD3; CD3⁺), natural killer cells (NK; NK1.1⁺), macrophages (Mφ; CD11b⁺F4/80⁺), granulocytic cells (Gran; CD11b⁺Gr-1⁺), and dendritic cells (DC; CD11c⁺MHCII⁺) per milligram of tumor. D) Quantification of CD86 expression by IT DCs. E) Quantification of DCs in tdLN. F,G) Quantification of PD-1⁺ expression by CD8⁺ and CD4⁺ cells in tumor-draining lymph node. Data are represented as mean ± SEM (n = 5). Multiple comparisons among groups were determined using one-way ANOVA followed by a posthoc test. P-value: *p < 0.05, **p < 0.01, ***p < 0.001.

cGAMP for use as antitumor therapeutics, such as ADU-S100.^[6a] Here, we designed an NP system to overcome the delivery barriers intrinsic to hydrophilic, anionic molecules such as CDNs that require cytoplasmic delivery to enable their function.

Previous efforts for IT delivery of CDNs centralized around encapsulation-based strategies whereby the CDN was housed inside the NP. For instance, liposomes^[19a,22] and polymeric NPs such as polymersomes,^[11] poly lactic-co-glycolic acid,^[23]

and acetalated dextran^[24] have been used for the IT administration of CDNs. These formulations typically rely on intrinsic elements of the synthesized material (e.g., pH responsiveness, endosomal disruption) for effective delivery. Depending on the formulation and batch, the amount of CDN may vary, especially as hydrophilic molecules are difficult to encapsulate with complete fidelity, and their storage stability can be compromised. We present a two-component dendrimer system that is avidly

internalized by cells and requires only simple mixing that is tuned to incorporate almost all CDN molecules, which has potential for scale-up. We,^[13b] and others,^[13a] have previously used PAMAM dendrimers as nucleic acid delivery systems, which is facilitated by electrostatic interactions between the cationic dendrimer and anionic nucleic acid. We modified dendrimers with polypeptide moieties with a dual-purpose function to enhance the cationic nature of the dendrimer by virtue of additional amines while simultaneously attenuating the toxicity originating from unmodified PAMAM dendrimers. This was achieved using a heterobifunctional linker that permits amide bond formation with the dendrimer and Michael addition with the thiol of polypeptide motifs of lysine, arginine, histidine, or combinations thereof. Successful conjugation was confirmed by ¹H-NMR and reflected by the increased size of all polypeptide-modified dendrimers and changes in surface charge (Figure 1). Histidine-containing formulations were less positively charged than their lysine or arginine counterparts at physiological pH due to the lower affinity for protons, resulting in partial protonation. This was further reflected by the greater complexation of ADU-S100 using D-CR3 compared to that of unmodified dendrimer (Figure 2 and Figure S10, Supporting Information). A combination of the increased amine groups from polypeptide-modified dendrimer and cationicity was theorized to be responsible for our observations, whereby D-CR3 could electrostatically entrap the most CDN-F as arginine has the highest pKa values (pKa of side chain = 12.48, 10.53, and 6.00, respectively, for arginine, lysine, and histidine). This is beneficial as less dendrimer is required to deliver the same dose of CDN-F, relative to other formulations.

Differential activation of IRF3 and NF-κB was observed when we screened our formulations *in vitro* (Figure 3). Greater activation of IRF3 was seen with NP formulations compared to equimolar concentrations of free ADU-S100, particularly beyond 250 nm. Dendrimer formulations containing arginine were found to be the most potent inducers of IRF3 and NF-κB, implying that these particles were internalized effectively and successfully delivered ADU-S100 to the cytoplasm. The activation of IRF3, which is downstream of STING, leads to transcription of IFN-Is and NF-κB signaling further elicits proinflammatory mediator activation.^[25] Indeed, modification of dendrimers with arginine has been described to improve the transfection efficiency while maintaining biocompatibility,^[26] matching our observations. NP formulations were differentially internalized into immune cells in a modification-dependent manner (Figure 3D). D-CH3 formulations were less efficiently internalized than D-CR3 and D-CK3, which would explain the lower IRF3 activation despite the potent endosomal escape properties of histidine.^[27] Lysine-modified dendrimers were internalized to a greater extent but were less potent activators of IRF3 compared to arginine-modified dendrimers. This may be due to the lower number of CDN delivered per dendrimer molecule, which may affect overall uptake and endosomal escape capacities. The mixture of arginine and lysine was well internalized and potently activated IRF3 and NF-κB; however, this formulation was more cytotoxic than the arginine alone.

Based on our *in vitro* data, we took forward the D-CR3 formulation, featuring high CDN complexation and biocompatibility, for *in vivo* evaluation. Previous reports demonstrated that high

doses of IT delivered CDN (up to 20 μg) induced tumor regression; however, the efficacy is severely diminished at lower doses.^[28] Here, we demonstrated that our NP formulation prevented growth of a poorly immunogenic murine melanoma model using 0.5 μg of ADU-S100, an effect that was further augmented when used in combination with anti-PD-1 (Figure 4). Interestingly, we observed that a low dose of free ADU-S100, particularly used in combination with anti-PD-1, was able to attenuate tumor growth, although less effective than the D-CR3-ADU. It is known that the intensity of STING signaling has a notable effect on the type and magnitude of the immune response. Low-dose IT administration of ADU-S100 was found to be more immunogenic than ablative (over 100 μg) doses and was optimal for combination with immune checkpoint blockade (ICB).^[19b] Even by potentially dosing with immunogenic amounts of free ADU-S100, our NPs were still able to improve antitumor responses compared to ADU-S100. Notably, without anti-PD-1, D-CR3-ADU was still able to attenuate tumor growth and to a much greater extent than equivalent free ADU-S100 alone. Indeed, the efficacy of our NP is comparable to that of other electrostatic polymeric NP-CDN formulations^[29] despite using lower CDN dose.

These observations led us to dive deeper into the mechanism underpinning antitumor efficacy. A decrease of proliferating cells and an increase of CD8⁺ T-cell infiltration was observed when ADU-S100 was delivered using D-CR3 compared to tumors treated with free ADU-S100, which are hallmarks of antitumor immune activation and induction of an immunogenic TME (Figure 5). This was further corroborated by the upregulation of the immune checkpoint molecule PD-L1 on tumor cells, which is known to occur in response to IFN-β^[30]—a direct downstream product of STING signaling—or IFN-γ produced by tumor-infiltrating T-cells.^[31] This suggests that increased STING signaling within the TME, facilitated by the D-CR3, resulted in greater production of IFNs such as IFN-β, leading to greater CD8⁺ T-cell infiltration and PD-L1 expression. Indeed, the improved therapeutic outcome seen with the inclusion of anti-PD-1 may be in part due to the reduced immunosuppressive PD-1/PD-L1 interactions that would otherwise occur upon STING-mediated upregulation of PD-L1.

In addition, flow cytometry analysis of the tumor immune infiltrate (Figure 6) confirmed an increase in CD8⁺/CD4⁺ T-cell and CD8⁺ T-cell/T_{reg} ratios in the D-CR3-ADU-treated groups compared with ADU-S100-treated or untreated tumors. Increased tumoral T_{reg} presence is a negative clinical prognostic indicator across a broad range of cancers,^[32] and thus our T-cell-related observations were encouraging. Interestingly, the number of NK cells was higher in all treated groups compared to untreated tumors, but significantly higher (twofold change) in the tumors treated with D-CR3-ADU. It has been shown that mobilization of NK cells in response to STING agonism can induce tumor regression independently of CD8⁺ T-cells and is a direct consequence of IFN-I production.^[33] A significant increase in activated granulocytic cells was evident in all treatment groups, which is consistent with the notion that granulocytes, particularly neutrophils, are among the first responders that migrate to the site of inflammation—in this case induced by STING activation. Interestingly, a trend of increase in the number of macrophages (CD11b⁺ F4/80⁺) and DCs (CD11c⁺

MHC-II⁺) compared to untreated tumors has only been observed in groups treated with anti-PD-1, which may be responsible for the improved efficacy witnessed when ADU-S100 was combined with anti-PD-1, given the role of DCs and macrophages in STING-mediated antitumor efficacy.^[34] Moreover, increased expression of the activation marker CD86 was evident on DCs within the TME treated with free ADU-S100 or complexed using D-CR3. Taken together, these immunological data show that D-CR3-ADU administration can remodel the TME to a more inflamed and immunoactive environment. Interestingly, we observed an increase in the presence of DCs in the tdLN-treated mice, which was most pronounced in D-CR3-ADU-treated mice. This suggests that a higher level of antigen presentation may have taken place as more DCs migrated from the TME to the tdLN to then cross-present to and prime CD8⁺ T-cells.

4. Conclusion

In the current study, we describe a library of polypeptide-modified dendrimers that can be used to effectively deliver CDN in vitro and in vivo. We found that arginine-modified dendrimers permit higher CDN complexation efficiency compared to nonmodified dendrimers. Our data show that D-CR3-ADU formulations are efficiently internalized into THP-1 cells, resulting in the activation of IRF3 and NF- κ B, and present lower toxicity than nonmodified dendrimers. In vivo results demonstrated that IT delivery of the D-CR3-ADU formulation in combination with anti-PD-1 induced strong tumor regression in a murine melanoma model. This polypeptide-modified dendrimer-based system can serve as a platform for efficient delivery of STING agonists in poorly immunogenic tumors, providing new opportunities for combination cancer therapy.

5. Experimental Section

Materials: All reagents and solvents were purchased from Sigma Aldrich unless otherwise stated. Polypeptides (H-Cys-Arg-Arg-Arg-NH₂, H-Cys-Lys-Lys-Lys-NH₂, and H-Cys-His-His-His-NH₂) were obtained from CPC Scientific with a purity of at least 90%. Generation 5 PAMAM dendrimer was purchased from Dendritech. Fluorescent CDN (Ap-8-Fluo-AET-Gp) was obtained from Biolog, Inc.

Fluorescent Labeling of Dendrimer: G5 PAMAM dendrimer was fluorescently tagged with AlexaFluor 594 carboxylic acid, succinimidyl ester (AF594) at 1:0.5 molar ratio (PAMAM dendrimer:AF594). Briefly, 14.22 μ L of AF594 at 10 mg mL⁻¹ in dimethylformamide (DMF) was mixed with 10 mg PAMAM dendrimer in 0.1 M bicarbonate buffer (pH 8.5) and reacted for 1 h at room temperature in the dark. Fluorescent dendrimers were washed with PBS and recovered by centrifugal filtration (10 kDa MWCO Amicon Ultra-0.5 mL Centrifugal Filters, Millipore) at 14 000 \times g for 10 min at 4 $^{\circ}$ C.

Synthesis of Polypeptide-Modified Dendrimers: PAMAM dendrimer was modified with bifunctional SM(PEG)₂ linker (Thermo Fisher), whereby 10 mg of dendrimer was dissolved in 500 μ L of 0.1 M phosphate buffer at pH 7.5 and 500 μ L PBS containing 19 mg of SM(PEG)₂ was added dropwise. The mixture was allowed to react for 30 min at room temperature. The dendrimer was then mixed with equimolar SM(PEG)₂ to polypeptide ratio and reacted at room temperature for 3 h. The polypeptide-modified dendrimer was purified by dialysis against PBS for 2 days at 4 $^{\circ}$ C. For structural analysis, modified dendrimers were freeze dried, dissolved in D₂O, and analyzed by ¹H-NMR, and recorded using a 400 MHz Varian NMR spectrometer (NMR Instruments, Clarendon Hills, IL).

Quantification of the Ratio of Peptides per Dendrimer by UV-Vis Spectroscopy: NanoDrop 2000c (Thermo Scientific, Tewksbury, MA) was used to characterize the polypeptide-modified dendrimer. Absorbance at 275 nm was used to determine the ratio of peptide to dendrimer. Because the fluorescent dendrimer also absorbs at 275 nm, the equation that follows was used to deconvolute the signals from each component (dendrimer or peptide) and obtain the peptide-to-dendrimer ratio (Equation (1)). The individual absorption coefficients were calculated from the respective UV-vis standard curves.

$$A_{\text{Dend-F \& Peptide}} = A_{\text{Dend-F}} + A_{\text{Peptide}} \quad (1)$$

$$\epsilon_{\text{Dend-F \& Peptide}} \times C_{\text{Dend-F \& Peptide}} = \epsilon_{\text{Dend-F}} \times C_{\text{Dend-F}} + \epsilon_{\text{Peptide}} \times C_{\text{Peptide}} \quad (2)$$

$$C_{\text{Dend-F \& Peptide}} = C_{\text{Dend-F}} \quad (3)$$

$$\frac{C_{\text{peptide}}}{C_{\text{Dend-F}}} = \frac{\epsilon_{\text{Dend-F \& Peptide}} - \epsilon_{\text{Dend-F}}}{\epsilon_{\text{Peptide}}} \quad (4)$$

Equation (1) is the peptide-to-dendrimer ratio calculation.

Biophysical Characterization of Polypeptide-Modified Dendrimers: To assess CDN complexation, different fluorescent CDN (Ap-8-Fluo-AET-Gp) to dendrimer ratios (w/w) between 0.5:1 and 64:1 were studied. Dendrimer-CDN complexes were freshly prepared; for example, to form 100 μ L of D-CR3 polyplexes, 50 μ L of CDN at 0.05 mg mL⁻¹ was mixed with 50 μ L of D-CR3 at 0.8 mg mL⁻¹. The dendrimer solution was added to CDN solution, pipette mixed, and incubated at room temperature for 10 min. Dendrimer-CDN polyplexes were loaded in 4% E-Gel Precast Agarose Gels (Thermo Fisher), run following the manufacturer's instructions, and visualized in fluorescence mode. The size and surface charge were determined by DLS and zeta potential measurements, respectively. Polyplexes were prepared as previously described and after 10 min of incubation at room temperature, 100 μ L of dendrimer was diluted with 900 μ L of PBS and analyzed using a Zetasizer Nano ZS equipped with a He-Ne laser ($\lambda = 633$ nm) at a scattering angle of 137 $^{\circ}$ (Malvern Instruments Ltd, United Kingdom).

CDN Loading Efficiency: Dendrimer-CDN complexes were freshly prepared as previously reported. To form 100 μ L of D-CR3-CDN polyplexes, 50 μ L of CDN at 0.05 mg mL⁻¹ was mixed with 50 μ L of D-CR3 at 0.8 mg mL⁻¹. To form 100 μ L of dendrimer-CDN polyplexes, 50 μ L of CDN at 0.05 mg mL⁻¹ was mixed with 50 μ L of unmodified dendrimer at 3.2 mg mL⁻¹. Noncomplexed CDN-F molecules were purified by centrifugal filtration (10 kDa MWCO Amicon Ultra-0.5 mL Centrifugal Filters, Millipore) at 14 000 \times g for 10 min at 4 $^{\circ}$ C and quantified by fluorescence ($\lambda_{\text{ex}} = 490$; $\lambda_{\text{em}} = 530$) using a multimodal plate reader (TECAN).

Cell Lines: *Mus musculus* skin melanoma (B16-F10, from ATCC) was maintained in Dulbecco's minimum essential medium (DMEM) supplemented with 10% fetal bovine serum (FBS), 100 U mL⁻¹ penicillin, and 100 μ g mL⁻¹ streptomycin, 2 mM L-glutamine. Human monocyte THP-1 Dual cells and THP-1 Dual KO-STING cells (InvivoGen) were maintained in RPMI 1640 supplemented with 10% FBS, 2 mM L-glutamine, 25 mM HEPES, 100 μ g mL⁻¹ Normocin, Zeocin, 10 μ g mL⁻¹ Blasticidin (InvivoGen), and 100 U mL⁻¹ penicillin and 100 μ g mL⁻¹ streptomycin. All cell lines were maintained in a humidified incubator at 37 $^{\circ}$ C, 5% CO₂.

In Vitro Evaluation of IRF and NF- κ B Pathways: Human monocyte THP-1 Dual cells and THP-1 Dual KO-STING cells were seeded in 96-well plates at 1 \times 10⁵ cells per well and incubated with the different dendrimer NP formulations or free CDN at CDN concentrations ranging from 0 to 500 nM. At 24 h post-treatment, IRF activity was examined using the QUANTI-Luc reagent (InvivoGen) and NF- κ B activity was determined using the QUANTI-Blue reagent (InvivoGen) according to the manufacturer's instructions.

Cell Viability: Cell viability was assessed using the MTS assay (Promega) as instructed by the manufacturer. After 24 h treatment with varying dendrimer-CDN NP formulations, MTS reagent was added to the cells to achieve a final MTS concentration of 20% (v/v). Cells were incubated at 37 $^{\circ}$ C, 5% CO₂ up to 2 h and absorbance was measured at 490 nm using a multimodal plate reader (TECAN).

Cellular Uptake: THP-1 Dual cells were seeded in 12-well plates at 5×10^5 cells per well and treated with fluorescent polypeptide-modified dendrimer at a concentration equivalent to 125 nM CDN. After 2 h at 37 °C, 5% CO₂, excess NPs were removed by washing with PBS and cells were collected by centrifugation. Following fixation with 1% (w/v) paraformaldehyde, cells were analyzed by flow cytometry using a BD LSRFortessa flow cytometer (BD Biosciences).

In Vivo Therapeutic Efficacy: Female C57BL/6 mice (6–8 weeks old) were purchased from Charles River. All mouse procedures were conducted at the Hale Building for Transformative Medicine and Koch Institute for Integrative Cancer Research at the Massachusetts Institute of Technology (MIT) under the protocol approved for this study by the Institutional Animal Care and Use Committee (IACUC). To induce tumors, 5×10^5 B16-F10 cells in 100 µL of Hanks' balanced salt solution (HBSS) were injected subcutaneously into the right flank of the mice. Upon reaching 50–100 mm³, tumors were intratumorally injected with 30 µL of PBS containing D-CR3-CDN polyplexes or free CDN (0.5 µg). Mice were injected four times with treatments spaced 4 days apart. Mice receiving ICB were injected intraperitoneally with 100 µg of anti-PD-1 (clone RMP1.14, Bio X Cell) 24 h post IT injection. The tumor size was measured every other day via caliper measurements, and the tumor volume was calculated using the equation $V = (L \times W \times H) / \pi \div 6$. Body weight was measured contemporaneously with tumor volume. Mice were euthanized when tumors reached a volume of 1000 mm³ or for otherwise poor body condition.

Analysis of Immune Infiltrate: B16-F10 tumors were harvested, chopped, and digested in a solution of HBSS supplemented with collagenase I, II, and IV (100 ng mL⁻¹), and DNase I (1 µg mL⁻¹) for 2 h at 37 °C. TdLNs were harvested and mechanically dissociated. Single-cell suspensions of tumors and tdLNs were filtered through a 40 µm nylon cell strainer. Tumor cells were further treated with ACK Lysing Buffer (Gibco). Cells were counted and stained with fluorescent antibodies at a concentration of 1×10^6 cells mL⁻¹ in 100 µL cell-staining buffer (BioLegend). Intracellular staining was performed using a FoxP3 Staining Buffer Set (Miltenyi) according to the manufacturer's protocol. The following anti-mouse antibodies were used for flow cytometry were purchased from BioLegend: CD45 APC-Cy7 (clone 30-F11), NK-1.1 BV710 (clone PK136), FOXP3 PE (clone MF-14) IFN-γ BV421 (clone XMG1.2), CD279 (PD-1) FITC (clone 29 F.1A12), CD45 BV785 (clone 30-F11), CD11b BV421 (clone M1170), Gr-1 APC-Cy7 (clone RB6-8C5), CD8a BV421 (clone 53-6.7), CD86 BV510 (clone GL-1), CD206 PE (clone C068C2), and MHCII BV605 (clone M5/114.15.2) CD11c APC (clone N418). The following anti-mouse antibodies were purchased from BD Biosciences: CD3 BB700 (clone 17A2), CD4 BUV395 (clone GK1.5), CD8a BUV737 (clone 53-6.7), F4/80 BUV395 (clone T45-2342), CD103 BUV395 (clone M290), and CD80 BUV737 (clone 16-10A1). Live cells were gated using LIVE/DEAD (Thermo Fisher) aqua (cat. no. L34966), green (cat. no. L34970), or NIR (cat. no. L34976). Stained cells were analyzed by flow cytometry using a BD LSRFortessa flow cytometer (BD Biosciences) and all data were analyzed using FlowJo software (FlowJo LLC).

Immunohistochemistry, Immunofluorescence, and Imaging: B16-F10 tumors were resected kept in 10% (v/v) formalin for a minimum of 24 h and then in 70% (v/v) ethanol until processing. H&E as well as expression of Ki-67, CD8, and PD-L1 protein was assessed by immunohistochemistry (IHC) from histological sections (5 µm) of tumors. H&E staining was performed using standard protocols. For protein expression, paraffin-embedded sections were deparaffinized, rehydrated, and washed in distilled water. Antigen retrieval was then performed in citrate buffer (pH 6.0) at 125 °C for 5 min. To quench endogenous peroxidase activity, samples were incubated with 3% (v/v) H₂O₂ for 5 min at room temperature and washed with PBS-Tween (PBS-T). The samples were then blocked with blocking buffer consisting of 10% (v/v) donkey serum, 1% (w/v) BSA in PBS-T for 60 min at room temperature. Sections were then incubated with anti-mouse CD8a (Thermo Fisher, cat. no. PA5-81344) or anti-mouse PD-L1 (Proteintech, cat. no. 66248-1-Ig) overnight at 4 °C in a humidified chamber. After rinsing with PBS-T, samples were incubated with either goat antirabbit AF594 (abcam, cat. no. ab150080) or goat antimouse AF488 (Jackson ImmunoResearch, cat. no. 115-543003) for 2 h at room

temperature in the dark. The slides were washed with PBS-T, stained with Hoescht 33342 (Thermo Fisher), washed again with PBS-T, and mounted using ProLong Diamond antifade mountant (Thermo Fisher). For Ki-67 expression, sections were run using a LabVision Autostainer 360 (Thermo Fisher) following an automated protocol using a polymer-based antibody detection system (Vector Laboratories) and visualization with 3,3'-diaminobenzidine. H&E and Ki-67 images were obtained using an Aperio AT2 slide scanner (Leica Biosystems) and fluorescence images were captured using a Nikon Ti-E microscope and were processed with ImageJ software.

Statistical Analysis: Statistical analyses were conducted using Graph-Pad Prism 8 (GraphPad Software). All data are reported as mean ± SEMs. For in vitro experiments, a minimum of $n = 3$ biological replicates were used per condition in each experiment. Pairwise comparisons were performed using Student *t*-tests. Multiple comparisons among groups were determined using one-way ANOVA followed by a posthoc test. For in vivo experiments, a minimum of $n = 5$ biological replicates were used per condition in each experiment. Multiple comparisons among groups were determined using Kruskal–Wallis test with uncorrected Dunn's test. Kaplan–Meier survival curve statistical analysis was determined using the two-tailed Mantel–Cox test. No specific preprocessing of data was performed prior to statistical analyses. Differences between groups were considered significant at *p*-values below 0.05 (**p* < 0.05, ***p* < 0.01, ****p* < 0.001).

Supporting Information

Supporting Information is available from the Wiley Online Library or from the author.

Acknowledgements

The authors thank the Hale Building for Transformative Medicine for the assistance with animal housing. The authors thank Swanson Biotechnology Center at the Koch Institute for Integrative Cancer Research at the Massachusetts Institute of Technology (MIT) for assistance with animal experiments and facilities, especially the microscopy, flow cytometry, and histology cores. The authors thank the Department of Comparative Medicine at MIT. The authors thank G. Paradis for FACS assistance with Cancer Center Support (FACS core). The authors thank Kathleen S. Cormier and Charlene Condon for histology and immunohistochemistry assistance. The authors thank Takeda Pharmaceuticals for provision of ADU-S100.

Conflict of Interest

The authors declare no conflict of interest.

Data Availability Statement

Research data are not shared.

Keywords

dendrimer nanoparticles, immunotherapy, intratumoral delivery, melanoma, stimulator of interferon genes agonist

Received: January 4, 2021

Revised: March 10, 2021

Published online:

- [1] T. Shekarian, S. Valsesia-Wittmann, J. Brody, M. C. Michallet, S. Depil, C. Caux, A. Marabelle, *Ann. Oncol.* **2017**, *28*, 1756.
- [2] a) P. Gao, M. Ascano, Y. Wu, W. Barchet, Barbara L. Gaffney, T. Zillinger, A. A. Serganov, Y. Liu, R. A. Jones, G. Hartmann, T. Tuschl, D. J. Patel, *Cell* **2013**, *153*, 1094; b) L. Sun, J. Wu, F. Du, X. Chen, Z. J. Chen, *Science* **2013**, *339*, 786.
- [3] a) X. Zhang, H. Shi, J. Wu, X. Zhang, L. Sun, C. Chen, Z. J. Chen, *Mol. Cell* **2013**, *51*, 226; b) E. J. Diner, D. L. Burdette, S. C. Wilson, K. M. Monroe, C. A. Kellenberger, M. Hyodo, Y. Hayakawa, M. C. Hammond, R. E. Vance, *Cell Rep.* **2013**, *3*, 1355.
- [4] a) S. Yum, M. Li, A. E. Frankel, Z. J. Chen, *Annu. Rev. Cancer Biol.* **2019**, *3*, 323; b) J. Kwon, S. F. Bakhoun, *Cancer Discovery* **2020**, *10*, 26.
- [5] a) H. Ishikawa, Z. Ma, G. N. Barber, *Nature* **2009**, *461*, 788; b) S.-R. Woo, M. B. Fuertes, L. Corrales, S. Spranger, M. J. Furdyna, M. Y. K. Leung, R. Duggan, Y. Wang, G. N. Barber, K. A. Fitzgerald, M.-L. Alegre, T. F. Gajewski, *Immunity* **2014**, *41*, 830.
- [6] a) L. Corrales, L. H. Glickman, S. M. McWhirter, D. B. Kanne, K. E. Sivick, G. E. Katibah, S. R. Woo, E. Lemmens, T. Banda, J. J. Leong, K. Metchette, T. W. Dubensky, Jr., T. F. Gajewski, *Cell Rep.* **2015**, *11*, 1018; b) T. Ohkuri, A. Kosaka, K. Ishibashi, T. Kumai, Y. Hirata, K. Ohara, T. Nagato, K. Oikawa, N. Aoki, Y. Harabuchi, E. Celis, H. Kobayashi, *Cancer Immunol. Immunother.* **2017**, *66*, 705; c) B. A. Flood, E. F. Higgs, S. Li, J. J. Luke, T. F. Gajewski, *Immunol. Rev.* **2019**, *290*, 24.
- [7] B. R. Huck, L. Kotzner, K. Urbahns, *Angew. Chem., Int. Ed.* **2018**, *57*, 4412.
- [8] T. W. Dubensky, D. B. Kanne, M. L. Leong, *Therap. Adv. Vaccines* **2013**, *1*, 131.
- [9] a) R. Zhang, M. M. Billingsley, M. J. Mitchell, *J. Control. Release* **2018**, *292*, 256; b) D. J. Irvine, E. L. Dane, *Nat. Rev. Immunol.* **2020**, *20*, 321.
- [10] S. T. Koshy, A. S. Cheung, L. Gu, A. R. Graveline, D. J. Mooney, *Adv. Biosyst.* **2017**, *1*, 1600013.
- [11] D. Shae, K. W. Becker, P. Christov, D. S. Yun, A. K. R. Lytton-Jean, S. Sevimli, M. Ascano, M. Kelley, D. B. Johnson, J. M. Balko, J. T. Wilson, *Nat. Nanotechnol.* **2019**, *14*, 269.
- [12] G. Bozzuto, A. Molinari, *Int. J. Nanomed.* **2015**, *10*, 975.
- [13] a) L. Palmerston Mendes, J. Pan, V. P. Torchilin, *Molecules* **2017**, *22*, 1401; b) J. Conde, N. Oliva, M. Atilano, H. S. Song, N. Artzi, *Nat. Mater.* **2016**, *15*, 353.
- [14] a) E. Vacas-Córdoba, N. Climent, F. J. De La Mata, M. Plana, R. Gómez, M. Pion, F. García, M. Á. Muñoz-Fernández, *Nanomedicine* **2014**, *9*, 2683; b) S. R. Bonam, A. Areti, P. Komirishetty, S. Muller, in *Pharmaceutical Applications of Dendrimers* (Eds.: A. Chauhan, H. Kulhari), Elsevier, Amsterdam **2020**, p. 233.
- [15] F. Abedi-Gaballu, G. Dehghan, M. Ghaffari, R. Yekta, S. Abbaspour-Ravasjani, B. Baradaran, J. E. N. Dolatabadi, M. R. Hamblin, *Appl. Mater. Today* **2018**, *12*, 177.
- [16] R. Duncan, L. Izzo, *Adv. Drug Deliv. Rev.* **2005**, *57*, 2215.
- [17] a) N. Segovia, P. Dosta, A. Cascante, V. Ramos, S. Borrós, *Acta Biomater.* **2014**, *10*, 2147; b) P. Dosta, N. Segovia, A. Cascante, V. Ramos, S. Borrós, *Acta Biomater.* **2015**, *20*, 82; c) R. Nunez-Toldra, P. Dosta, S. Montori, V. Ramos, M. Atari, S. Borros, *Acta Biomater.* **2017**, *53*, 152.
- [18] a) P. Dosta, I. Tamargo, V. Ramos, S. Kumar, D. W. Kang, S. Borros, H. Jo, *Adv. Healthcare Mater.* **2021**, <https://doi.org/10.1002/adhm.202001894>; b) P. Dosta, C. Demos, V. Ramos, D. W. Kang, S. Kumar, H. Jo, S. Borros, *Cardiovasc. Eng. Technol.* **2021**, *12*, 114.
- [19] a) S. T. Koshy, A. S. Cheung, L. Gu, A. R. Graveline, D. J. Mooney, *Adv. Biosyst.* **2017**, *1*, 1600013; b) K. E. Sivick, A. L. Desbien, L. H. Glickman, G. L. Reiner, L. Corrales, N. H. Surh, T. E. Hudson, U. T. Vu, B. J. Francica, T. Banda, G. E. Katibah, D. B. Kanne, J. J. Leong, K. Metchette, J. R. Bruml, C. O. Ndubaku, J. M. McKenna, Y. Feng, L. Zheng, S. L. Bender, C. Y. Cho, M. L. Leong, A. van Elsas, T. W. Dubensky, S. M. McWhirter, *Cell Rep.* **2018**, *25*, 3074.
- [20] N.-P. Rudqvist, K. A. Pilonis, C. Lhuillier, E. Wennerberg, J.-W. Sidhom, R. O. Emerson, H. S. Robins, J. Schneck, S. C. Formenti, S. Demaria, *Cancer Immunol. Res.* **2018**, *6*, 139.
- [21] Z. Cheng, T. Dai, X. He, Z. Zhang, F. Xie, S. Wang, L. Zhang, F. Zhou, *Signal Transd. Targeted Therapy* **2020**, *5*, 91.
- [22] a) T. Nakamura, H. Miyabe, M. Hyodo, Y. Sato, Y. Hayakawa, H. Harashima, *J. Control Release* **2015**, *216*, 149; b) N. Cheng, R. Watkins-Schulz, R. D. Junkins, C. N. David, B. M. Johnson, S. A. Montgomery, K. J. Peine, D. B. Darr, H. Yuan, K. P. McKinnon, Q. Liu, L. Miao, L. Huang, E. M. Bachelder, K. M. Ainslie, J. P. Ting, *JCI Insight* **2018**, *3*, e120638.
- [23] S. Chattopadhyay, Y. H. Liu, Z. S. Fang, C. L. Lin, J. C. Lin, B. Y. Yao, C. J. Hu, *Nano Lett.* **2020**, *20*, 2246.
- [24] R. Watkins-Schulz, P. Tiet, M. D. Galovic, R. D. Junkins, C. Batty, E. M. Bachelder, K. M. Ainslie, J. P. Y. Ting, *Biomaterials* **2019**, *205*, 94.
- [25] T. Abe, G. N. Barber, *J. Virol.* **2014**, *88*, 5328.
- [26] a) J. S. Choi, K. Nam, J.-y. Park, J.-B. Kim, J.-K. Lee, J.-s. Park, *J. Controlled Release* **2004**, *99*, 445; b) T. Okuda, A. Sugiyama, T. Niidome, H. Aoyagi, *Biomaterials* **2004**, *25*, 537.
- [27] Y. Wen, Z. Guo, Z. Du, R. Fang, H. Wu, X. Zeng, C. Wang, M. Feng, S. Pan, *Biomaterials* **2012**, *33*, 8111.
- [28] J. Fu, D. B. Kanne, M. Leong, L. H. Glickman, S. M. McWhirter, E. Lemmens, K. Metchette, J. J. Leong, P. Lauer, W. Liu, K. E. Sivick, Q. Zeng, K. C. Soares, L. Zheng, D. A. Portnoy, J. J. Woodward, D. M. Pardoll, T. W. Dubensky, Jr., Y. Kim, *Sci. Transl. Med.* **2015**, *7*, 283ra52.
- [29] D. R. Wilson, R. Sen, J. C. Sunshine, D. M. Pardoll, J. J. Green, Y. J. Kim, *Nanomed. Nanotechnol. Biol. Med.* **2018**, *14*, 237.
- [30] A. Garcia-Diaz, D. S. Shin, B. H. Moreno, J. Saco, H. Escuin-Ordinas, G. A. Rodriguez, J. M. Zaretsky, L. Sun, W. Hugo, X. Wang, G. Parisi, C. P. Saus, D. Y. Torrejon, T. G. Graeber, B. Comin-Anduix, S. Hu-Lieskovan, R. Damoiseaux, R. S. Lo, A. Ribas, *Cell Rep.* **2017**, *19*, 1189.
- [31] A. Thiem, S. Hesbacher, H. Kneitz, T. di Primio, M. V. Heppt, H. M. Hermanns, M. Goebeler, S. Meierjohann, R. Houben, D. Schrama, *J. Exp. Clin. Cancer Res.* **2019**, *38*, 397.
- [32] B. Shang, Y. Liu, S.-j. Jiang, Y. Liu, *Sci. Rep.* **2015**, *5*, 15179.
- [33] C. J. Nicolai, N. Wolf, I. C. Chang, G. Kirn, A. Marcus, C. O. Ndubaku, S. M. McWhirter, D. H. Raulet, *Sci. Immunol.* **2020**, *5*, eaaz2738.
- [34] R. E. Vatner, E. M. Janssen, *Mol. Immunol.* **2019**, *110*, 13.